molecules

MDPI

Article

Crystal Structure and Optical Properties of ZnO:Ce Nano Film

Mei Xin [1,2]

[1] School of Physics and Materials Engineering, Dalian Nationalities University, Dalian 116600, China; xinmei_dl@126.com
[2] Liaoning Key Laboratory of Optoelectronic Films and Materials, Dalian Nationalities University, Dalian 116600, China

Abstract: ZnO and cerium-doped ZnO on a glass substrate have been prepared by the sol–gel method using the spin coating technique and water bath growth process. Ce-doping concentration on film structure, morphology, and optical properties is investigated. The result indicated that the hexagonal wurtzite ZnO with high crystalline quality formed on the substrate. The crystal parameters a and c decreased, crystal size increased, and the compressive strain formed after Ce-doping. Formed un-, 3%, 6%, 12% Ce-doped ZnO film has a spherical shape with a size between 8.6–31, 14–52, 18–56, and 20–91 nm, respectively. All films had good absorption of 300–400 nm ultraviolet light, in particular, the absorption of near ultraviolet (370–400 nm) increased after doping of Ce. The transmittance of light between 400–800 nm decreased with Ce-doping concentration. The band gap energy increased after Ce-doping reaching better optical behavior for preparing ZnO heterostructured thin-film. All film emitted intense blue emission under 375 nm excitation at room temperature. This indicated the film can have application in optoelectronic devices.

Keywords: ZnO:Ce; thin film; sol-gel; nanocrystal; optical properties; blue emission; color purity

Citation: Xin, M. Crystal Structure and Optical Properties of ZnO:Ce Nano Film. *Molecules* **2022**, *27*, 5308. https://doi.org/10.3390/molecules27165308

Academic Editor: Barbara Panunzi

Received: 28 July 2022
Accepted: 19 August 2022
Published: 20 August 2022

1. Introduction

Zinc oxide (ZnO) has a band-gap width of 3.37 eV at room temperature (RT) and an exciton energy of 60 meV. ZnO has excellent chemical stability because of its hexagonal wurtzite structure at normal temperatures leading to a large Coulomb force for its positive and negative electron pairs [1]. ZnO is environmentally friendly, inexpensive, and abundant in nature and intrinsic defects such as oxygen vacancies or Zn interstitials are mostly on the surface of ZnO causing visible emissions [2,3]. All these unique properties make ZnO application in the ultraviolet (UV) and blue source and have efficient exciton emission [4]. ZnO has also attracted research interest for its applications in optoelectronic applications by forming homo, pn junction, and heterogeneous materials [5–7], and gas detection [8,9]. ZnO is generally an n-type semiconductor that usually forms a heterojunction LED with GaN, SiC, and other p-type semiconductors, and is used in optoelectronic devices [10]. For some of their specific application requirements, ZnO film requires specific structural features, morphology, and optical band gaps [11]. Doping is a significant and effective way to improve the physical properties of ZnO thin films [12]. Cerium-doped ZnO is widely used due to its unique properties including visible-light-emitting devices [13,14], catalytic characteristic [15–17], new diluted magnetic [18], spintronics [19,20] and gas sensor [21]. Various synthesis techniques have been used to prepare ZnO nanoparticles, such spray pyrolysis [22], RF magnetron sputtering [23], solid-state reaction [24], solution method [25,26], electrospinning [27] co-precipitation [28], sol–gel [29,30]. In this study, we report the Ce concentration on structural, morphological, and optical properties of sample films deposited by the sol–gel method combining the spin coating technique and water bath growth. This process can reduce spin coating time, simplicity, and uniformity film on glass substrates. Few reports about affect Ce concentration on the crystal structure of ZnO:Ce film. In this work, the effect of Ce-doping on the crystal structure and the optical properties of ZnO:Ce were studied in detail.

2. Experimental Process

2.1. The Deposition of Un- and Ce-Doped ZnO Film on Glass Substrates

All reactants were reagent grade (AR). Ce-doped sample added 3%, 6%, 12% of $Ce(NO_3)_35H_2O$ to solution. The deposition processes as Figure 1.

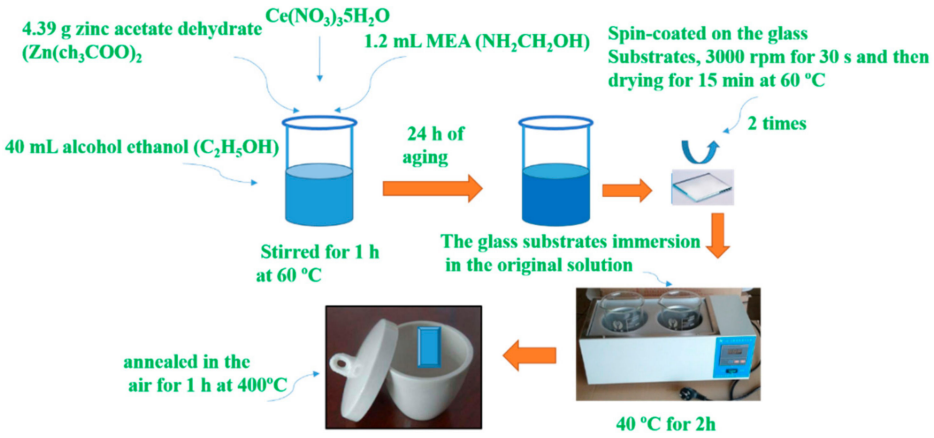

Figure 1. Schematic diagram for the deposition of un- and Ce-doped ZnO film on glass substrates.

2.2. Film Characterization

The structure and morphology were examined by using an XRD (SHIMADZU-6000) and SEM (Hitachi S4800). UV/vis transmittance and absorption of the sample were performed using UV-3600 SHIMADZU spectrophotometer. PL spectra were measured by HITACHI F-4600 spectrophotometer. All measurements were performed at room temperature.

3. Results and Discussion

3.1. XRD and SEM Analysis

Figure 2 shows the XRD patterns of un-, 3%, 6% and 12% Ce-doped ZnO film. The films are well matched with hexagonal wurtzite ZnO (JCPDS 36-1451) [29]. The strongest diffraction peak is obtained at 3% Ce-doped sample and the diffraction peak intensity decreases with further increasing of Ce contents. When Ce-doping ratio is 12%, CeO_2 impurity appeared (2θ–29°) marked as * in Figure 2 [16,29]. Ce-doped ZnO film oriented along (101) crystallographic plane. The lattice constants calculated using:

$$\frac{1}{d_{hkl}^2} = \frac{4}{3}\left(\frac{h^2 + hk + k^2}{a^2}\right) + \frac{l^2}{c^2} \quad (1)$$

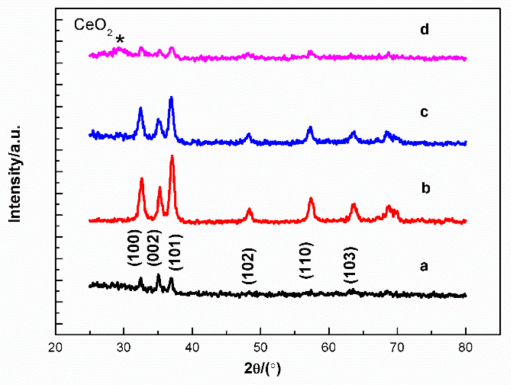

Figure 2. XRD patterns of un-(**a**), 3% (**b**), 6% (**c**) and 12% (**d**) Ce-doped ZnO film.

The crystallite size (D) is calculated using the Debye–Scherrer's formula for the average calculated date of the (100), (002) and (101) diffraction peaks [31].

$$D = \frac{0.89\lambda}{\beta cos\theta} \quad (2)$$

$$\varepsilon_{zz} = \frac{(c - c_0)}{c_0} \times 100\% \quad (3)$$

where ε_{zz} is along the c axis, c_0 and c is the lattice parameter of un- and Ce-doped ZnO film.

The crystal size increased and lattice constant decreased after Ce doping (Table 1). The ionic radii of Ce^{4+} and Ce^{3+} (0.087 and 0.115 nm, respectively) be larger than that of the Zn^{2+} ion of 0.074 nm [1]. The compressive strain is formed after doping of Ce. Changes in crystal structure after doping Ce indicate that Ce is incorporated into the ZnO matrix. SEM result indicated that film morphology of un-, 3%, 6% and 12% Ce-doped ZnO film diameter range in 8.6–31, 14–52, 18–56 and 20–91 nm, respectively (Figure 3). A hundred particles were selected and measured by Image J software. The 3% and 6% Ce-doped samples appear with a spherical morphology. There is a local agglomeration in the undoped and 12% Ce-doped sample, and the uniformity of the film after doping 3% and 6% Ce is obtained. In our previous work, the morphology of doped ZnO was changed from granular to rod when doping concentration is larger than 1% deposited on glass substrate by similar method [32–34]. However, in this work, the sample morphology do not change after larger than 1% Ce-doping, as well as lattice constant decreased after doping of larger ionic radii of Ce indicating the unique properties of Ce ions. It is maybe due to the dominant compressive strain on ZnO lattice caused by Ce enclosed in grain boundaries and prevents the growth further along the growing crystal orientation [35,36].The particle size increased after doping of Ce, consistent with the calculated size trend.

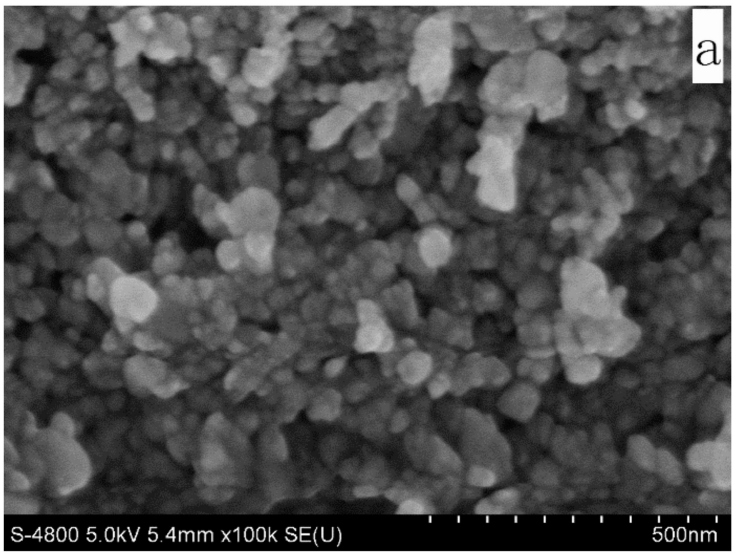

Figure 3. *Cont.*

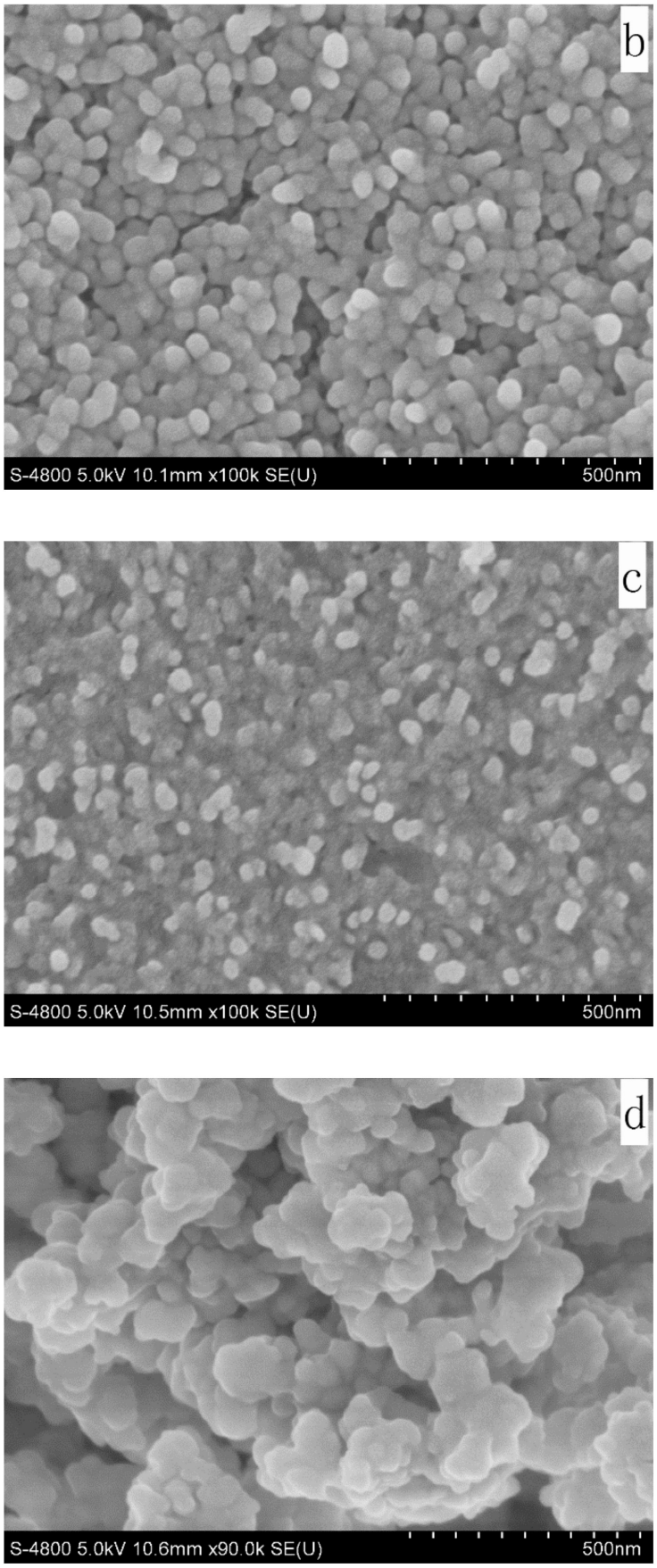

Figure 3. SEM of un-(**a**) 3% (**b**) 6% (**c**) 12% (**d**) Ce-doped (**b**) ZnO thin film.

Table 1. Lattice constant and diameter of undoped and Ce-doped ZnO thin film.

Molar Ratio of Ce (%)	Lattice Constant			ε_{zz}	Debye–Scherrer's D (nm)	SEM G (nm)
	a	*c*	*c*/*a*			
0	0.2995	0.4815	1.61	0	14.93	8.6–31
3	0.2972	0.4781	1.61	−0.70	17.94	14–52
6	0.2989	0.4806	1.61	−0.20	16.03	18–56
12	0.2989	0.4784	1.60	−0.50	23.79	20–91

3.2. Optical Properties

The film completely absorbs the ultraviolet (UV) light and transmits the visible light. The visible light transmittance decreases with increasing of Ce content (Figure 4). Numerous factors can influence film visible light transmittance. In our experiment, the decreased visible light transmittance is maybe due to crystal size increased after Ce-doping. UV-vis absorbance of un-and Ce-doped ZnO film displayed as Figure 5. The absorbance peak appears at about 300 nm. The absorption of near ultraviolet (370–400 nm) is stronger than the undoped one after doping of Ce ions. Optical gap values for un- and Ce-doped ZnO using the well-known Equation (4)

$$\alpha h\nu = A\left(h\nu - E_g\right)^{1/2} \quad (4)$$

The value of absorption coefficient (a) is intercepted between 314–376 nm for calculating the band gap (E_g). The band gap of undoped, doping of 3%, 6% and 12% Ce ZnO is found to be 3.43, 3.49, 3.46 and 3.51 eV, respectively. The band gap increases after doping of Ce (Figure 6). The possible reason may relate to strain. The compressive strain widened band gap [37]. In addition, because of the Burstein–Moss effect also make the band gap widened [38]. The increase in the optical band gap brings it closer to the band gap width of p-type semiconductor materials and reaching better optical behavior for preparing ZnO heterostructured thin-film [39].

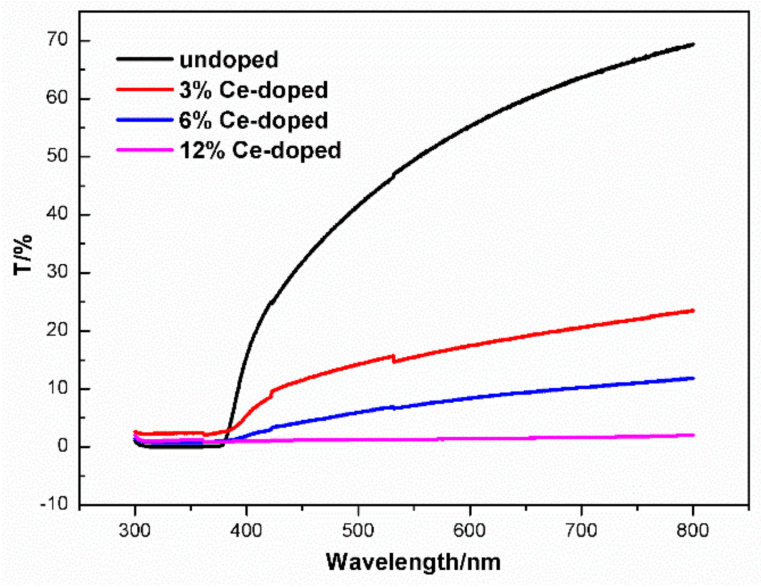

Figure 4. UV-vis optical transmittance of un-and Ce-doped ZnO films.

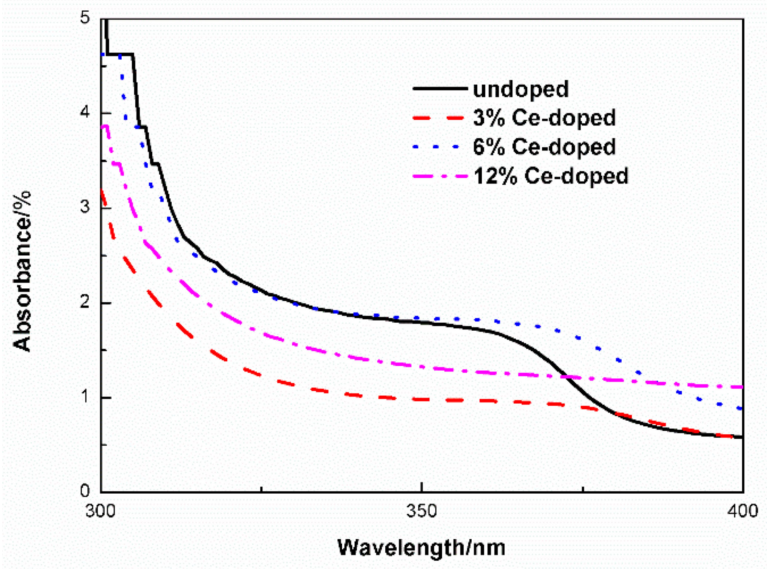

Figure 5. UV-vis absorbance of un-and Ce-doped ZnO films.

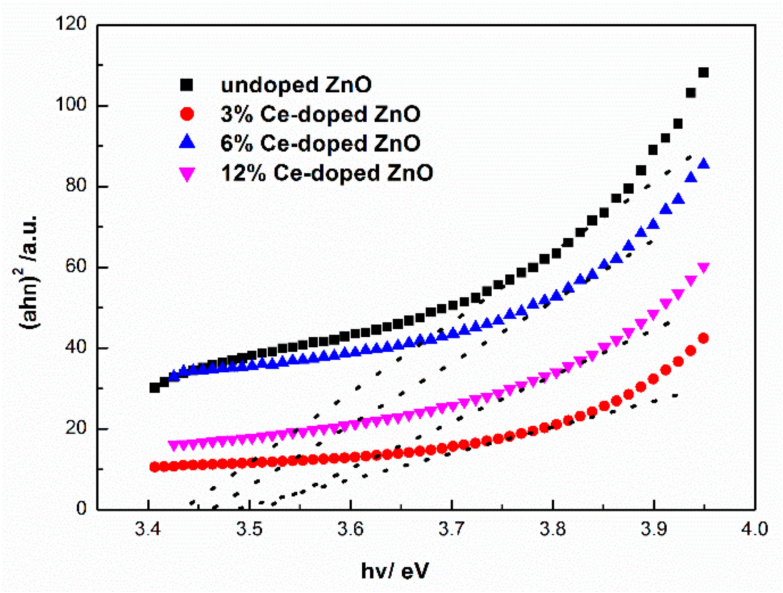

Figure 6. Optical band gap (a is intercepted between 314–376 nm) of un- and different Ce-doped ZnO films.

The PL emission spectra of un-and different Ce-doped ZnO film under 375 nm excitation are shown in Figure 7. All films have emission peaks at about 424 and 442 nm. An emission of 424 nm is assigned to the recombination of the Zn interstitial levels to the top of the valence band; 442 nm emission is attributed to the recombination of O vacancies to the valence band [32]. CIE-1931 chromaticity coordinates of samples is (0.1518, 0.0594), (0.1517, 0.0602), (0.1518, 0.0603), (0.1519, 0.0598) for undoped and 3%, 6%, 12% Ce-doped ZnO, respectively (Figure 8). The color purity was calculated using [40]

$$\text{Color Purity} = \frac{\sqrt{(x_s - x_i)^2 + (y_s - y_i)^2}}{\sqrt{(x_d - x_i)^2 + (y_d - y_i)^2}} \times 100\% \quad (5)$$

where (x_s, y_s) are the coordinates of a sample point; in our experiment all of the sample coordinates are basically the same, and the value is (0.152, 0.060), (x_d, y_d) are the coordinates of the dominant wavelength, in our experiment dominant wavelength at 442 nm, its coordinate is (0.1756, 0.0053) and (x_i, y_i) are the coordinates of the CIE coordinates of white

illuminant point is (0.310, 0.316). The calculated colour purity is 89%, indicating that this material has potential application in blue light sources.

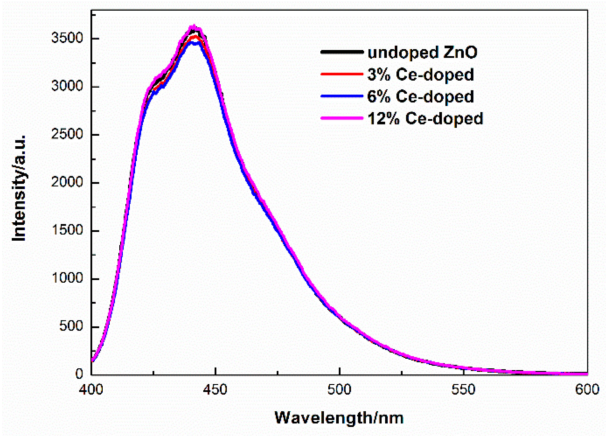

Figure 7. PL of un- and different Ce-doped ZnO films (λ_{ex} = 375 nm).

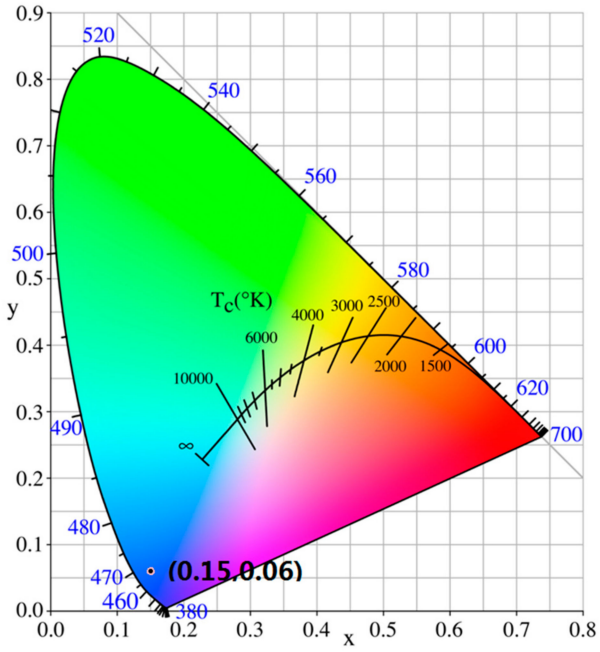

Figure 8. CIE-1931 chromaticity coordinates of samples excited under 375 nm.

4. Conclusions

In summary, undoped, Ce-doped ZnO films deposited on glass substrates were synthesized by sol–gel method contained spin coating and water bath growth technique. The Ce incorporation on the crystal structure and optical properties of un- and Ce-doped ZnO film was investigated. XRD results indicated that all films formed a hexagonal wurtzite ZnO crystal structure, the lattice constant decreased, crystal size increased, and compressive strain formed after Ce-doping, indicating the Ce incorporated into ZnO crystal. The presence of spherical type was confirmed by SEM. Room temperature UV–vis and PL spectra showed strong absorption in the near UV region and the absorption of near ultraviolet (370–400 nm) increased after doping of Ce ions. Optical transmittance of visible light was reduced with increasing Ce-doping content. The band gap energy increased after Ce-doping. Intense blue emission with a color purity of 89% was observed under 375 nm excitation. ZnO:Ce film has potential applications in the near ultraviolet (n-UV) LED light conversion materials and a blue light source.

Funding: This research received no external funding.

Institutional Review Board Statement: Not applicable.

Informed Consent Statement: Not applicable.

Data Availability Statement: Not applicable.

Acknowledgments: Thanks to the assistance of the key laboratory of Dalian Nationalities University and the financial support of college students' innovation projects.

Conflicts of Interest: The authors declare no conflict of interest.

References

1. Chen, Z.W.; Yao, C.B.; Han, Y.; Bao, S.B.; Jiang, G.Q.; Cai, Y. Synthesis, structure and femtosecond nonlinear absorption properties of Ce-ZnO films. *Appl. Surf. Sci.* **2020**, *502*, 144133. [CrossRef]
2. Kim, H.H.; Park, S.; Ko, K.; Yim, S.; Kang, J.; Choi, W.K. Blue Light Emitting Diodes based on Bright Quasi-Type-II ZnO@1-Aminopyrene Hybrid Quantum Dots with a Long Operation Life. *Adv. Opt. Mater.* **2022**, *2022*, 2200601. [CrossRef]
3. López-López, J.; Tejeda-Ochoa, A.; López-Beltrán, A.; Herrera-Ramírez, J.; Méndez-Herrera, P. Sunlight photocatalytic performance of zno nanoparticles synthesized by green chemistry using different botanical extracts and zinc acetate as a precursor. *Molecules* **2022**, *27*, 6. [CrossRef] [PubMed]
4. Chelouche, A.; Touam, T.; Tazerout, M.; Djouadi, D.; Boudjouan, F. Effect of Li codoping on highly oriented sol-gel Ce-doped ZnO thin films properties. *J. Lumin.* **2017**, *188*, 331–336. [CrossRef]
5. Jung, Y.-I.; Noh, B.-Y.; Lee, Y.-S.; Baek, S.-H.; Kim, J.H.; Park, I.-K. Visible emission from Ce-doped ZnO nanorods grown by hydrothermal method without a post thermal annealing process. *Nanoscale Res. Lett.* **2012**, *7*, 43. [CrossRef] [PubMed]
6. Park, W.I.; Yi, G.C.; Kim, J.W.; Park, S.M. Schottky nanocontacts on ZnO nanorod arrays. *Appl. Phys. Lett.* **2003**, *82*, 4358–4360. [CrossRef]
7. Fradi, K.; Bouich, A.; Slimi, B.; Chtourou, R. Towards improving the optoelectronics properties of $MAPbI_{3(1-x)}B_{3x}$/ZnO heterojunction by bromine doping. *Optik* **2022**, *249*, 168283. [CrossRef]
8. Kannadasan, N.; Shanmugam, N.; Sathishkumar, K.; Cholan, S.; Poonguzhali, R.; Viruthagiri, G. Synthesis of Ce^{4+} ions doped ZnO electrode as a sensor for hydrogen peroxide. *J. Mater. Sci. Mater. Electron.* **2014**, *25*, 5137–5143. [CrossRef]
9. Zhu, L.; Zeng, W. Room-temperature gas sensing of ZnO-based gas sensor: A review. *Sens. Actuators A Phys.* **2017**, *267*, 242–261. [CrossRef]
10. Ünal, D.; Varol, S.F.; Brault, J.; Chenot, S.; Al Khalfioui, M.; Merdan, Z. Improved performance of near UV-blue n-ZnO/p-GaN heterostructure LED with an AlN electron blocking layer. *Microelectron. Eng.* **2022**, *262*, 111830. [CrossRef]
11. Duan, J.X.; Wang, H.; Huang, X.T. Synthesis and characterization of ZnO ellipsoid-like nanostructures. *Chin. J. Chem. Phys.* **2007**, *20*, 613–618. [CrossRef]
12. Malimabe, M.A.; Motloung, S.V.; Motaung, T.E.; Koao, L.F. Effects of Eu^{3+} co-doping on the structural and optical properties of Ce^{3+} doped ZnO powder synthesized by chemical bath deposition method. *Phys. B Condens. Matter* **2020**, *579*, 411890. [CrossRef]
13. Shi, Q.; Wang, C.; Li, S.; Wang, Q.; Zhang, B.; Wang, W.; Zhang, J.; Zhu, H. Enhancing blue luminescence from Ce-doped ZnO nanophosphor by Li doping. *Nanoscale Res. Lett.* **2014**, *9*, 480. [CrossRef]
14. Rani, S.; Lal, B. ZnO nanophosphor Co doped with Ce, Eu and Tb. *Opt. Quantum Electron.* **2020**, *52*, 328. [CrossRef]
15. Gong, H.C.; Zhong, J.F.; Zhou, S.M.; Zhang, B.; Li, Z.H.; Du, Z.L. Ce-induced single-crystalline hierarchical zinc oxide nanobrushes. *Superlattices Microstruct.* **2008**, *44*, 183–190. [CrossRef]
16. Rodríguez-Peña, M.; Flores-Carrasco, G.; Urbieta, A.; Rabanal, M.E.; Fernández, P. Growth and characterisation of ZnO micro/nanostructures doped with cerium for photocatalytic degradation applications. *J. Alloys Compd.* **2020**, *820*. [CrossRef]
17. Jian, S.; Tian, Z.; Zhang, K.; Duan, G.; Yang, W.; Jiang, S. Hydrothermal Synthesis of Ce-doped ZnO Heterojunction Supported on Carbon Nanofibers with High Visible Light Photocatalytic Activity. *Chem. Res. Chin. Univ.* **2021**, *37*, 565–570. [CrossRef]
18. Wen, J.Q.; Zhang, J.M.; Qiu, Z.G.; Yang, X.; Li, Z.Q. The investigation of Ce doped ZnO crystal: The electronic, optical and magnetic properties. *Phys. B Condens. Matter* **2018**, *534*, 44–50. [CrossRef]
19. Kayani, Z.N.; Chaudhry, T.; Riaz, S.; Naseem, S. Dielectric and Magnetic Properties of Rare-Earth Metal Ce-Doped ZnO Thin Films. *J. Electron. Mater.* **2020**, *49*, 3114–3123. [CrossRef]
20. Khan, R.; Althubeiti, K.; Zulfiqar; Afzal, A.M.; Rahman, N.; Fashu, S.; Zhang, W.; Khan, A.; Zheng, R. Structure and magnetic properties of (Co, Ce) co-doped ZnO-based diluted magnetic semiconductor nanoparticles. *J. Mater. Sci. Mater. Electron.* **2021**, *32*, 24394–24400. [CrossRef]
21. Lu, W.; Zhu, D.; Xiang, X. Synthesis and properties of Ce-doped ZnO as a sensor for 1,2-propanediol. *J. Mater. Sci. Mater. Electron.* **2017**, *28*, 18929–18935. [CrossRef]
22. Sofiani, Z.; Derkowska, B.; Dalasiński, P.; Wojdyła, M.; Dabos-Seignon, S.; Lamrani, M.A.; Dghoughi, L.; Bała, W.; Addou, M.; Sahraoui, B. Optical properties of ZnO and ZnO:Ce layers grown by spray pyrolysis. *Opt. Commun.* **2006**, *267*, 433–439. [CrossRef]
23. García-Méndez, M.; Segura, R.R.; Coello, V.; Guerra, E.M.; Bedoya-Calle, Á. The influence of Ce doping on the structural and optoelectronic properties of RF-sputtered ZnO films. *Opt. Quantum Electron.* **2015**, *47*, 2637–2648. [CrossRef]

24. Letswalo, M.L.A.; Reddy, L.; Balakrishna, A.; Swart, H.C.; Ntwaeaborwa, O.M. The role of sulfate ions on distinctive defect emissions in ZnO:Ce^{3+} nanophosphors - A study on the application in color display systems. *J. Lumin.* **2021**, *240*, 118462. [CrossRef]
25. Sa-nguanprang, S.; Phuruangrat, A.; Karthik, K.; Thongtem, S.; Thongtem, T. Tartaric acid-assisted precipitation of visible light-driven Ce-doped ZnO nanoparticles used for photodegradation of methylene blue. *J. Aust. Ceram. Soc.* **2020**, *56*, 1029–1041. [CrossRef]
26. Singh, P.; Kumar, R.; Singh, R.K. Fabrication of Co- and Ce-doped ZnO nanoparticles: A structural, morphological and optical properties investigation. *Appl. Nanosci.* **2020**, *10*, 1231–1241. [CrossRef]
27. Li, F.M.; Li, X.B.; Ma, S.Y.; Chen, L.; Li, W.Q.; Zhu, C.T.; Xu, X.L.; Chen, Y.; Li, Y.F.; Lawson, G. Influence of Ce doping on microstructure of ZnO nanoparticles and their acetone sensing properties. *J. Alloys Compd.* **2015**, *649*, 1136–1144. [CrossRef]
28. Shukla, S.K.; Agorku, E.S.; Mittal, H.; Mishra, A.K. Synthesis, characterization and photoluminescence properties of Ce^{3+}-doped ZnO-nanophosphors. *Chem. Pap.* **2014**, *68*, 217–222. [CrossRef]
29. Khanlary, M.R.; Hajinorozi, A.; Baghshahi, S. Influence of Ce Doping Concentration on the Structural and Optical Properties of Sol–Gel Derived ZnO:Ce Nanostructures. *J. Inorg. Organomet. Polym. Mater.* **2015**, *25*, 1521–1528. [CrossRef]
30. Kumawat, A.; Sharma, A.; Chattopadhyay, S.; Misra, K.P. Temperature dependent photoluminescence in sol-gel derived ce doped zno nanoparticles. *Mater. Today Proc.* **2021**, *43*, 2965–2969. [CrossRef]
31. Kammoun, S.; Ghoul, J. El Structural and optical investigation of Co-doped ZnO nanoparticles for nanooptoelectronic devices. *J. Mater. Sci. Mater. Electron.* **2021**, *32*, 7215–7225. [CrossRef]
32. Xin, M. Growth temperature on ZnO:Al thin films morphology and optical properties. *Surf. Eng.* **2021**, *37*, 1476–1483. [CrossRef]
33. Xin, M. Optical properties of nanostructured ZnO:Eu film by sol–gel method. *Surf. Eng.* **2019**, *35*, 947–953. [CrossRef]
34. Xin, M.; Zhong, L.; Liu, D.; Yu, N. Superlattices and Microstructures Effect of Mn doping on the optical, structural and photoluminescence properties of nanostructured ZnO thin film synthesized by sol–gel technique. *SUPERLATTICES Microstruct.* **2014**, *74*, 234–241. [CrossRef]
35. Boufelgha, F.; Brihi, N.; Labreche, F.; Guendouz, H.; Barbadj, A. Enhanced of Blue and Green Emission by Ce–ZnO Thin Films Prepared by Sol–gel Technique. *Semiconductors* **2022**, *56*, 275–280. [CrossRef]
36. Shanmugam, N.; Cholan, S.; Kannadasan, N.; Sathishkumar, K.; Viruthagiri, G. Effect of polyvinylpyrrolidone as capping agent on Ce^{3+} doped flowerlike ZnS nanostructure. *Solid State Sci.* **2014**, *28*, 55–60. [CrossRef]
37. Xu, Z.; Hou, Q.; Guo, F.; Jia, X.; Li, C.; Li, W. Effects of strain on the optical and magnetic properties of Ce-doped ZnO. *Curr. Appl. Phys.* **2018**, *18*, 1465–1472. [CrossRef]
38. Xu, Z.; Hou, Q.; Guo, F.; Li, Y.; Liu, Y. Effect of strains on the optical and magnetic properties of Ce-doped ZnO with O or Zn vacancies. *J. Mater. Sci.* **2020**, *55*, 7390–7402. [CrossRef]
39. Ferhati, H.; Djeffal, F.; Bendjerad, A.; Saidi, A.; Benhaya, A. Post-annealing effects on RF sputtered all-amorphous ZnO/SiC heterostructure for solar-blind highly-detective and ultralow dark-noise UV photodetector. *J. Non. Cryst. Solids* **2021**, *574*, 121168. [CrossRef]
40. Zhao, J.; Gao, H.; Xu, H.; Zhao, Z.; Bu, H.; Cao, X.; He, L.; Yang, Z.; Sun, J. Structure and photoluminescence of Eu^{3+} doped Sr_2InTaO_6 red phosphor with high color purity. *RSC Adv.* **2021**, *11*, 8282–8289. [CrossRef]